Tribology International 220 (2026) 111956

Contents lists available at ScienceDirect

Tribology International

journal homepage: www.elsevier.com/locate/triboint

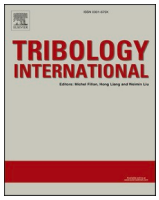

Full length article

Influence of carbide morphology and matrix hardness on the sliding wear behaviour of tool steels

Marko Sedlaček [a,*], Božo Skela [b], Bojan Podgornik [a]

[a] Institute of Metals and Technology, Lepi pot 11, Ljubljana 1000, Slovenia
[b] Impol R&R d.o.o., Partizanska ulica 38, Slovenska Bistrica 2310, Slovenia

ARTICLE INFO

Keywords:
Tool steel
Hardness
Sliding wear
Carbide fraction
Fracture toughness
Reciprocating sliding
Third-body abrasion

ABSTRACT

When using tool steels with martensitic microstructure, the hardness is regarded as one of the main criteria defining its wear properties. The premise is that the harder the material, the greater the sliding wear resistance. This is especially common when using tool steels, as the highest possible hardness is pursued, but the influence of the microstructure is often neglected. Presence of different carbides in terms of fraction, type and size (morphology) in martensitic matrix has different effects on wear, especially if matrix hardness changes. The objective of this study was to establish a correlation between the fraction and morphology of V and Cr-rich carbides in tool steel with its microstructure, fracture toughness, and overall influence on material sliding wear resistance. To achieve this, commercially available tool steels (Mat. No. 1.2379 cold work tool steel and modified Mat. No. 1.2367 hot work tool steel) were selected, exhibiting notably diverse microstructures, particularly in terms of carbide fraction and morphology. To enable a direct comparison, both steels underwent heat treatment to attain three distinct hardness levels: 45 + /-1 HRC, 49 + /-1 HRC, and 54 + /-1 HRC. Sliding wear resistance and behavior under various contact conditions were correlated with microstructure, specifically focusing on hard carbides. Additionally, the study examined the effect of wear particles being trapped within or removed from the tribological contact. It was observed that the sliding wear behavior is significantly influenced when the microstructure comprises a martensitic matrix with a higher fraction of carbides, particularly coarse eutectic M_7C_3 carbides, especially if the matrix hardness is insufficient. Matrix hardness plays a crucial role in preventing carbide detachment from the matrix. Plastic deformation of the tempered martensite matrix, along with carbide cracking and detachment from the matrix, was identified as contributing factors intensifying wear during the wear process.

1. Introduction

Tool steels are important for manufacturing cutting tools, molds, and dies because their high hardness, wear resistance, and thermal stability ensure precision, durability, and reliable performance under demanding operational conditions. Although tools' performance is determined by their microstructure and mechanical properties, the wear resistance of tool steels has traditionally been linked primarily to their hardness. It is widely accepted that higher hardness generally corresponds to improved wear resistance. It has also been shown that, for steels, pearlite and bainite do not exhibit such good wear resistance as a harder martensitic microstructure with carbides [1]. Additionally, a greater influence on abrasive wear comes from the hardness of the martensite than its volume fraction [2,3]. However, this approach overlooks the significant role played by microstructural features such as the type, size, morphology, and distribution of carbides within the tool steel matrix.

Microstructure and fraction of wear resistant carbides in steels is determined by processing history, heat treatment and especially by composition and alloying elements. In general, cold work tool steels are high carbon steels combined with high chromium content. They have high carbides fraction, possess an excellent wear resistance and non-deforming properties [4,5]. In one of the most widely used cold work tool steels, 1.2379 (AISI D2) only one type of solidification derived carbides formed during solidification M_7C_3 rich in chromium is present, at the same time showing great dependence of fracture toughness on the carbides orientation [6]. On the other hand, the typical carbon content in hot-work tool steels is relatively low (0.30–0.40 wt% C), resulting in significantly lower carbides fraction [5] and resistance to plastic

* Corresponding author.
E-mail address: marko.sedlacek@imt.si (M. Sedlaček).

https://doi.org/10.1016/j.triboint.2026.111956
Received 9 January 2026; Received in revised form 10 March 2026; Accepted 18 March 2026
Available online 22 March 2026

deformation, but still high wear resistance. This clearly shows that wear resistance of tool steels is not only hardness dependent.

Research in the field of microstructure effect and correlations to wear resistance of tool steels is quite extensively covered, comprising different approaches to the problem [7–16]. For example, study by Badisch and Mitterer [7] focused on the correlation between the hardness of the abrasive particles, volume fraction of primary carbides and abrasive wear resistance of high-speed steels. Study showed that the hardness of the abrasive material in relation to primary carbides plays an important role in terms of wear resistance. If the abrasive particles are harder than the primary carbides, properties of the matrix like hardness and ductility play a dominant role [8]. Research performed by Singh et al. [11], on the other hand indicated that by increasing tempering temperature during multiple tempering of 1.2379 cold work tool steel, coarsening of the carbides occurs, resulting in lower abrasive wear resistance of the material. The highest abrasive wear resistance observed for as-quenched steel was not attributed solely to higher hardness but mainly to martensitic microstructure with finer carbides. Research on dry sliding wear resistance of 1.2344 hot work tool steel (AISI H13) performed by Wei et al. [1] revealed difference in wear resistance depending on the contact conditions and tempering temperature. At low loads as-quenched samples and samples tempered at lower temperatures showed higher wear resistance, while at high loads tempering at 600°C provided the highest wear resistance [17].

The work by Leskovšek et al. [18] also exposed the importance of fracture toughness on the performance of tool steels, including wear resistance. It was shown that by designing combined hardness-fracture toughness tempering diagrams the best properties of tool steel for a given application can be obtained.

Although prior studies have emphasized that carbide's characteristics, alongside matrix hardness, substantially influence wear behavior of tool steels [19,20], gaps in terms of effect of carbide type and morphology as well as level of fracture toughness remain that necessitate further research and clarifications. Understanding the effect of carbides on the wear resistance will facilitate further design and maximizing potential of tool steels without necessarily focusing on high martensitic matrix hardness. It is of great interest to tribologically evaluate conventional tool steels to its full potential, as more exclusive materials are much more expensive and presents greater costs [9].

The objective of this study is to correlate the volume fraction and morphology of V- and Cr-rich carbides with the microstructure, fracture toughness, and abrasion resistance of two commercially available tool steels: Mat. No. 1.2379 (AISI D2) and a modified hot work tool steel Mat. No. 1.2367 (AISI H11 mod.). Furthermore, work is aimed at providing guidelines for obtaining best suited microstructure for a given tribological contact and contact conditions. Both materials were subjected to controlled heat treatments to produce three hardness levels: ~45 ± 1 HRC, ~49 ± 1 HRC, and ~54 ± 1 HRC. This approach isolates the effect of matrix hardness from carbide influence, facilitating a direct assessment of wear mechanisms under varying contact conditions.

2. Material and methods

2.1. Material

In our study two commercially available chromium type tool steels were used, one belonging to hot work tool steel group - modified Mat. No. 1.2367 with reduced Mo content and added Ni (modified AISI H11), denoted A and other to the cold work tool steel - Mat. No. 1.2379 (AISI D2) – denoted B. Both were delivered in a shape of hot forged and soft annealed plates, from which different specimens were machined. Hot work tool steel A is primarily used for tools used in the process of extrusion, forging and die casting of light metals and alloys, having good toughness, high working hardness and improved thermal conductivity. Cold work tool steel B is an excellent air hardening, high wear resistant tool steel. It is highly stable ledeburitic steel, with an option of tempering on secondary hardening peak [21]. Table 1 lists chemical composition of the steels used in this investigation.

2.2. Heat treatment

Heat treatment of the investigated tool steel specimens was conducted in IPSEN VTTC-324R horizontal vacuum furnace with high pressure gas quenching in nitrogen. The heat treatment parameters were chosen in such a way that three comparable hardness levels were obtained for both steels; level 1–54 ± 1 HRC, level 2–49 ± 1 HRC and level 3–45 ± 1 HRC. Each set of specimens was first austenitized for 20 min and quenched, followed by double 2 h tempering. After two stage preheating (650 °C and 850 °C) hot work tool steel specimens (A) were heated (@12 °C/min) to the final austenitizing temperature of 1030°C, soaked for 20 min and quenched in nitrogen gas at a quenching speed of 3 °C/s. The tempering sequence for hot work tool steel specimens consisted of first tempering cycle performed at 500 °C and subsequent tempering at 510 °C (level 1 hardness – A-1), 550 °C (level 2 hardness – A-2) and 615°C (level 3 hardness – A-3). For cold work tool steel specimens (B) final austenitizing temperature was 1020 °C, quenching speed 7.5 °C/s and the following double tempering sequences applied: 553 °C and 555 °C (level 1 hardness – B-1), 570 °C and 580 °C (level 2 hardness - B-2), and 590 °C and 600 °C (level 3 hardness - B-3). Table 2 summaries heat treatments performed and targeted hardness levels.

2.3. Hardness and fracture toughness

The hardness of the investigated samples was measured using the Rockwell-C method on a Rockwell 4JR (Instron B2000) hardness testing machine in accordance with the ISO 6508–1 standard. For each specimen, a minimum of three indentations were performed, and the average hardness value was calculated.

The matrix hardness of all tool steel specimens was determined according to the SIST EN ISO 6507–1 standard using an Instron Tukon 2100B Vickers microhardness tester with a test load of 5 N (HV0.05). On the other hand, instrumented nano-indentation testing was also employed to generate the hardness distribution maps across the microstructure. Nano-indentation was conducted using an Anton Paar NHT3 nanoindentation device, operating in the Quick Matrix indentation mode, with a 30 × 30 indentation matrix and a total of 900 individual measurements per specimen. The minimum spacing between indents was 4 μm, and the maximum applied load was 10.00 mN.

Fracture toughness testing was performed using circumferentially notched and fatigue pre-cracked tensile bar specimens, following the methodology proposed by Leskovšek et al. [22], which includes fatigue pre-cracking prior heat treatment, tensile loading until fracture and measurement of brittle fractured area. Tensile loading until fracture was conducted on an INSTRON 1255 universal testing machine with a crosshead speed of 1.0 mm/min. The nominal specimen diameter (D) was 10 mm, length (L) 100 mm, and precise axial alignment of the tensile load was ensured. Load-displacement data were continuously recorded during testing and load at fracture (P) identified. Following fracture, the diameter of the brittle fractured area (d) was measured, and the fracture toughness (K_{Ic}) was subsequently calculated using the Eq. (1):

$$K_{Ic} = \frac{P}{D^{3/2}} \bullet \left(-1.27 + 1.72 \bullet \frac{D}{d} \right) \quad (1)$$

A minimum of four test specimens were evaluated, and the average fracture toughness value was calculated.

2.4. Microstructure characterization

Specimens were metallographically prepared using standard procedures for tool steels, including sequential grinding and final polishing

Table 1
Chemical composition of the used steels (in mass %).

Chemical content (in mass %)		C	Si	Mn	Cr	Ni	Mo	V	Fe
Steel	Named								
Mat. No. 1.2367 mod.	A	0.36	0.3	0.5	4.9	1.51	1.94	0.66	Rest
Mat. No. 1.2379	B	1.41	0.35	0.2	11.1	-	0.76	0.85	Rest

Table 2
Heat treatments and targeted hardness levels for the investigated steels.

Sample Type	Material	Austenitization	Quenching Speed	Tempering Sequence	Target Hardness
A-1	Hot Work Tool Steel (mod. 1.2367)	1030°C/20 min	3 °C/s	500°C/2 h + 510°C/2 h	54 ± 1 HRC
A-2		1030°C/20 min	3 °C/s	500°C/2 h + 550°C/2 h	49 ± 1 HRC
A-3		1030°C/20 min	3 °C/s	500°C/2 h + 615°C/2 h	45 ± 1 HRC
B-1	Cold Work Tool Steel (1.2379)	1020°C/20 min	7.5 °C/s	553°C/2 h + 555°C/2 h	54 ± 1 HRC
B-2		1020°C/20 min	7.5 °C/s	570°C/2 h + 580°C/2 h	49 ± 1 HRC
B-3		1020°C/20 min	7.5 °C/s	590°C/2 h + 600°C/2 h	45 ± 1 HRC

with diamond paste. Microstructural features were revealed using a Nital etchant (5 mL HNO_3, 95 mL ethanol). The microstructure was first examined with an optical microscope (Nikon Microphot FXA) equipped with a Hitachi HV-C20A 3CCD video camera and image analysis software. Detailed microstructural investigation was conducted using a JEOL JSM-6500F field-emission scanning electron microscope (FE-SEM) and a ZEISS Crossbeam 550 FIB-SEM Gemini II. SEM imaging was performed in secondary electron imaging (SEI) mode with an accelerating voltage of 15 kV.

To quantify the size, distribution, and volume fraction of the most abundant surface carbides (critical for wear resistance), feature counting analysis was performed using INCA software. Measurements were conducted at various magnifications (500 ×, 2500 ×, 4000 × for Cr-rich carbides and 500 ×, 5000 × and 10000 × for V-rich carbides) depending on carbide size, on 10 randomly selected areas. The analysis was based on contrast differences between the matrix and carbides in backscattered electron (BSE) mode on polished specimens, as described in reference [23]. Vanadium-rich MC-type carbides appeared dark to black, while chromium-rich carbides, such as M_7C_3 and $M_{23}C_6$, exhibited a darker grey contrast and were primarily identified based on their size. Carbides were classified as follows: Solidification derived carbides (SDC): > 5 μm; Secondary carbides (SC): < 5 μm; Large secondary carbides (LSC): 1–5 μm; and Small secondary carbides (SSC): 0.1–1 μm. During automatic feature analysis, energy-dispersive X-ray spectroscopy (EDS) was simultaneously conducted for each detected particle to confirm its chemical composition (chromium-rich or vanadium-rich). To ensure statistical reliability and cover the full-size range of carbides, feature analysis of carbides was performed at different magnifications: 500 × , 2500 × , and 4000 × for Cr-rich carbides, and 10,000 × for V-rich carbides. This classification and methodology have been established and applied in previous studies [10,13].

Electron backscatter diffraction (EBSD) analysis was performed to investigate the crystallographic features of the microstructure and to further characterize carbide types within the martensitic matrix. The presence of retained austenite in heat-treated specimens was assessed using X-ray diffraction (XRD) with a PANalytical X'PERT 3040 diffractometer equipped with a rotating Cu anode (Cu-Kα: $\lambda_1 = 1.54059$ Å, $\lambda_2 = 1.54441$ Å). XRD measurements were performed at 40 kV and 45 mA, over a 2θ range of 20°–90°, with a step size of 0.02° s^{-1} using a linear detector. Bulk specimens were metallographically prepared prior to measurement and mounted with the polished surface oriented perpendicular to the incident X-ray beam. During data acquisition, the specimens were continuously rotated in-plane to enhance statistical averaging of grain orientations.

2.5. Tribological testing

To evaluate the influence of carbide fraction, size, and type on the sliding wear resistance of selected tool steels, reciprocating dry sliding tests were performed using a ball-on-flat contact configuration. All tests were conducted on polished disc specimens under dry sliding conditions at ambient temperature. A surface roughness of$Ra = 0.07$ μm was achieved through final polishing with diamond paste.

A 20 mm diameter ceramic Al_2O_3 ball (hardness: HV ~1700) was used as oscillating counter-body to impose dry reciprocating sliding conditions with a high hardness mismatch. These conditions are known to promote sliding wear with contributions from abrasive, adhesive, fatigue-related (delamination), and tribochemical/oxidative processes. However, some material transfer from the tool steel disc to the ceramic ball (adhesive wear) was also observed. The wear of the ceramic counter-body was not the focus of this study and was therefore not evaluated.

Two nominal loads of 30 N and 102 N were used in this investigation, corresponding to the nominal Hertzian contact pressure of 1.0 GPa and 1.6 GPa, respectively. The sliding distance was limited to 100 m. A reciprocating frequency of 15 Hz was applied, resulting in an average sliding speed of 0.12 m/s.

To assess the role of carbides and to analyze their influence as third-body wear particles during reciprocating sliding, an in-situ particle removal through a continuous air-blowing method was employed. As illustrated in Fig. 1a, the air nozzle was positioned near the contact zone to immediately remove any generated wear particles. Dehumidified compressed air was applied throughout the test to minimize the accumulation of wear particles. Fig. 1b demonstrates the successful removal of wear particles from the wear track after the test. For these tests, the lower load condition (1.0 GPa) was applied to minimize the potential interference of third-body effects. Specimens of the level 1 hardness group (54 ± 1 HRC) were used in order to reduce particle indentation and facilitate efficient removal of wear particles from the contact zone, thereby limiting third-body abrasion and promoting a micro-cutting–dominated wear regime.

Furthermore, specimens of the level 3 hardness group (45 ± 1 HRC) were further subjected to prolonged unidirectional sliding tests, using the same contact configuration, nominal contact pressure of 1.0 GPa and sliding speed of 0.12 m/s, but prolonging sliding distance to 200 m to allow full evolvement of the wear track including large and small carbides. Tests were aimed at identifying the effect of carbides on wear mechanism and damage evolution. The lowest hardness group specimens were selected to clearly observe and capture the most extensive microstructural damage induced by wear. By focusing on the softest material condition, the extent of deformation and wear-related changes was maximized, providing valuable insight into the wear mechanisms at

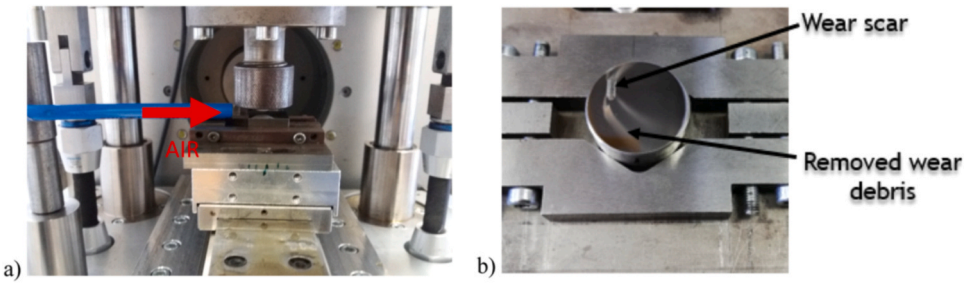

Fig. 1. a) Reciprocating sliding test rig with nozzle for air blowing method, b) indication of wear scar with removed wear particles.

their most critical stage.

During wear testing, the coefficient of friction was continuously recorded and both steady state and average coefficient of friction calculated. After the completion of the test wear volume was measured using a 3D optical microscope (Alicona Infinite Focus G4). Wear resistance was quantified in terms of wear coefficient k_W [mm^3/Nm], commonly calculated according to Eq. (2), where ΔV is the wear volume [mm^3], F is the normal load [N] and s is the sliding distance [m]. To ensure repeatability, a minimum of three test repetitions were performed for each contact condition.

$$k_W = \frac{\Delta V}{F \bullet s} \tag{2}$$

3. Results and discussion

3.1. Microstructure

The microstructure of the two investigated tool steels quenched and tempered to three different hardness levels exhibited the presence of various carbide types within a tempered martensitic matrix (Fig. 2). Carbide type and morphology in this investigation was primarily determined by steel chemical composition, with the same carbides being present within each steel grade, regardless of the heat treatment conditions and final hardness achieved after tempering. Therefore, only results from the level 2 hardness group (49 ± 1 HRC) will be presented and discussed in detail in this section.

The microstructure of the modified hot work tool steel A after quenching and tempering consists of a tempered martensitic matrix with a distribution of small undissolved carbides, as shown in Fig. 2a. Detailed microstructural analysis of material A revealed exclusively vanadium-rich MC-type carbides, clearly visible in BSE images at higher magnification (Fig. 2b) and further confirmed by EBSD analysis (Fig. 3c). EDS spectroscopy confirmed that carbides in tool steel A are vanadium-enriched, with moderate contents of molybdenum and chromium. Additionally, nitrogen was occasionally detected within these carbides, indicating the presence of vanadium-rich carbo-nitrides, being well in agreement with previous studies [23,24].

As illustrated in Fig. 2a-c, large solidification derived chromium-rich carbides (solidification-derived carbides) were not observed in tool steel A. This can be attributed to its low carbon content—more than 50% lower than for typical cold work tool steels—insufficient to promote the formation of massive solidification derived carbides.

The microstructure of cold work tool steel B is shown in Fig. 2d-f, revealing a high density of large solidification derived carbides alongside significant amounts of smaller secondary carbides (Fig. 2f). The

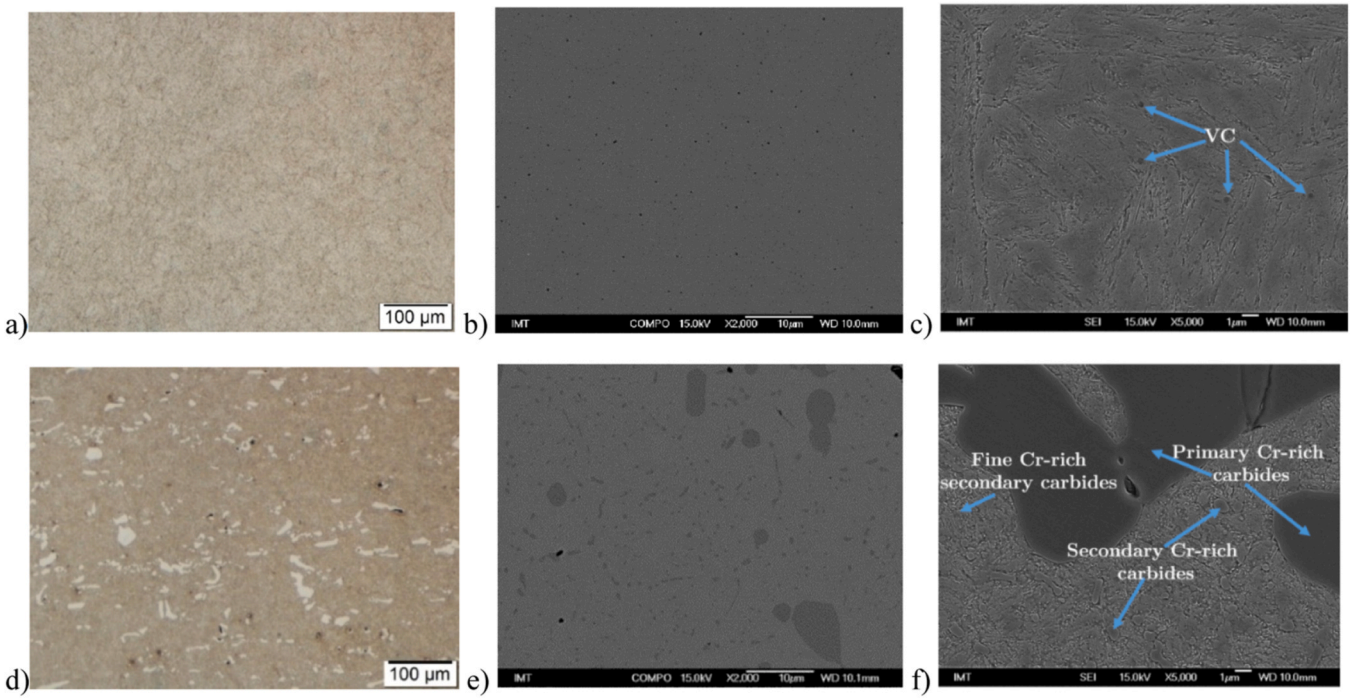

Fig. 2. Microstructure of quenched and tempered A-2 and B-2 tool steel specimens (hardness group 2; a, b, c A-2 & d, e, f B-2) showing martensite microstructure; a, d) optical micrograph of etched microstructure, b, e) BSE micrograph at 2.000 × magnification and c, f) SEI micrograph of etched microstructure at 5.000 × magnification.

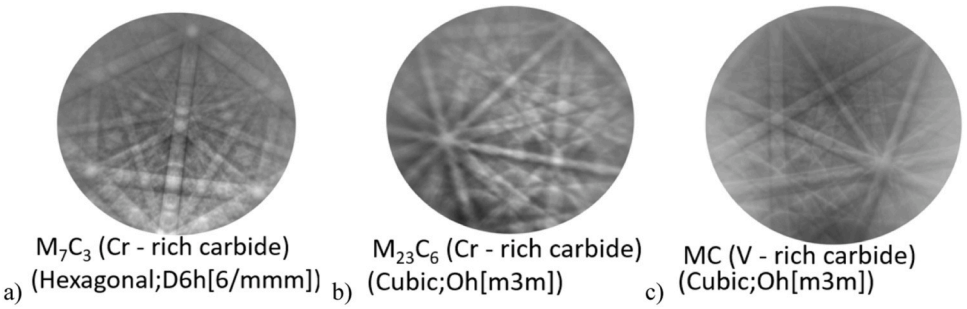

Fig. 3. SEM/EBSD characterization of carbides in quenched and tempered tool steels; a) EBSD pattern of Cr- rich carbides of M_7C_3 type, b) EBSD pattern of Cr- rich carbides of $M_{23}C_6$ type and c) EBSD pattern of V- rich carbides of MC type present in the tempered martensite matrix.

solidification derived carbides formed during solidification, confirmed by EBSD to be chromium-rich M_7C_3 with hexagonal structure (Fig. 3a), dominate the microstructure. High contents of carbon, chromium, and molybdenum in this steel promote the formation of massive solidification derived carbides during solidification, which remain undissolved even at high austenitizing temperatures [25] and are known to significantly enhance wear resistance of steels [26]. The distribution and size of these solidification derived carbides remain stable throughout the hardening process, with their volume fraction and size in 1.2379 cold work tool steels typically ranging from 7 to 15% [13] and 15–20 μm [26], respectively.

In the present study, tempering was performed at higher temperatures than typically recommended for 1.2379 steel grade, in order to achieve hardness levels comparable to the hot work tool steel. Higher tempering temperatures promoted the precipitation and coarsening of fine secondary carbides [14,27]. EBSD analysis confirmed that the secondary carbides are predominantly $M_{23}C_6$ with cubic crystal structure (Fig. 3b). Although smaller than the coarse M_7C_3 carbides formed during solidification, the secondary carbides are more uniformly distributed throughout the martensitic matrix. Elevated tempering temperatures also increased the iron content within both solidification derived and secondary carbides. Chromium carbide precipitation predominantly occurs at lower and intermediate tempering temperatures, while the precipitation of iron-rich carbides at higher tempering temperatures indicates the decomposition of martensite into ferrite and the formation of orthorhombic cementite (Fe_3C) [28]. Due to limitations in EBSD resolution, the crystallographic pattern of this phase could not be reliably detected.

Another important microstructural feature in high-alloy tool steels is retained austenite [14]. However, in the current study, austenitizing was performed at lower recommended temperatures, followed by immediate double tempering at temperatures above 500 °C. Consequently, the retained austenite fraction was substantially reduced, being below 1.5% for all the tempered specimens, as confirmed by XRD measurements.

3.2. Fraction and distribution of carbides

Results for the carbides volume fraction analysis of the investigated tool steels are summarized in Table 3. Cold work tool steel B shows considerably higher overall carbide fraction than hot work tool steel A, summing up at about 12% of total carbide content within the steel matrix. Notably, the fraction of solidification derived carbides (SDC) in tool steel B reached ~6%, which is consistent with values reported in previous studies [10]. Secondary carbides (SC) fractions, both large secondary carbides (LSC) and small secondary carbides (SSC), also align with reported values for this type of steel [10,13]. The minor variations observed in carbides fractions across specimens can be attributed to variations in chemical composition. Additionally, an increase in tempering temperature resulted in a slight increase in secondary carbide fractions, with LSC increasing from 2.7% to 3.0% and SSC increasing from 2.9% to 3.6% (Table 3).

Table 3
Fraction of detected Cr- and V- rich carbides in the investigated tool steel specimens based on INCA Feature analysis.

Specimen	Cr-rich C [%]			V-rich C [%]	Total [%]
	SDC	LSC	SSC		
A-1	/			0.41 + /- 0.09	0.41
A-2				0.42 + /- 0.12	0.42
A-3				0.45 + /- 0.06	0.45
B-1	6.04 + /-0.20	2.74 + /- 0.31	2.91 + /-0.36		11.69
B-2		3.02 + /- 0.87	3.34 + /-0.47		12.41
B-3		3.05 + /- 0.40	3.58 + /-0.55		12.67

SDC- solidification derived carbides; LSC- large secondary carbides; SSC- small secondary carbides

In contrast, hot work tool steel A exhibited a significantly lower overall carbide fraction, ranging from 0.41% to 0.45%. Primarily, only V-rich carbides were detected using the applied characterization techniques. These carbides correspond to the proeutectoid phase, whose fraction is mainly influenced by the austenitization temperature, which was identical for all hardness levels in this study. Although other chromium-based carbides, such as M_7C_3 and $M_{23}C_6$, are expected to be present in this type of tool steel [29–31], their size is typically below 0.5 μm [23], and thus their detection limited under the imaging and measurement conditions applied in this investigation.

Table 4 presents the mean diameter of the carbides identified in the investigated tool steels. The largest carbides were the solidification derived carbides (SDC) in tool steel B, with an average mean diameter of 9.7 ± 4.8 μm. Among the secondary carbides, large secondary carbides (LSC) had a mean diameter of approximately 2 μm, while small secondary carbides (SSC) exhibited an average mean diameter of about 0.6 μm across all specimens. For the V-rich proeutectoid carbides in tool steel A, the mean diameter was 0.2 μm, regardless of the tempering temperature applied.

The mean free path between carbides was also quantified and is reported in Table 5. In the hot work tool steel A, the V-rich carbides

Table 4
Average carbide diameter.

Average carbide diameter [μm] of V-rich carbides in tool steel A		
0.199 + /- 0.096		
Average carbide diameter [μm] of Cr-rich carbides in tool steel B		
SDC	LSC	SSC
9.697 + /- 4.844	1.917 + /- 0.866	0.604 + /- 0.174

SDC- solidification derived carbides; LSC- large secondary carbides; SSC- small secondary carbides

Table 5
Mean free path of carbides in martensite matrix.

Mean free path [μm] of V-rich carbides in tool steel A	
0.092 + /- 0.0489	
Mean free path [μm] of Cr-rich carbides in tool steel B	
SDC	LSC
5.122 + /- 2.665	0.366 + /- 0.199

SDC- SDC- solidification derived carbides; SSC- small secondary carbides

exhibited a mean free path of 0.092 ± 0.049 μm, indicating a very fine dispersion within the martensitic matrix. In contrast, the distribution of solidification derived carbides in the cold work tool steel B showed significantly larger mean free path, averaging at 5.122 ± 2.665 μm. Secondary carbides in tool steel B were more uniformly distributed, with the LSC mean free path measured at 0.366 ± 0.199 μm, and an even smaller spacing observed for SSC.

3.3. Hardness distribution

The hardness of the matrix phase in all investigated specimens was evaluated using the Vickers microhardness method. The results are presented in Table 6. A low indentation load of 5 g was selected to ensure that the measurements targeted only the matrix phase containing small secondary carbides, while avoiding the influence of coarse solidification derived carbides—particularly in tool steel B. As shown in Table 6, across all bulk hardness levels, tool steel A consistently exhibits higher matrix hardness values. Specifically, the matrix hardness reached up to 650 HV0.05 for specimen A-1, approximately 570 HV0.05 for specimen A-2, and around 500 HV0.05 for specimen A-3. In comparison, the matrix hardness values of tool steel B were 3–4% lower, as shown in Table 6.

The difference between Vickers and Rockwell hardness can be explained by considering the microstructural contributions to the bulk hardness. When bulk hardness is measured using the Rockwell-C method, the hardness readings are influenced by the presence of coarse solidification derived carbides, which possess significantly higher hardness than the surrounding matrix. As discussed earlier, the mean free path between these solidification derived carbides in tool steel B is approx. 5 μm, while the typical Rockwell-C indentation is substantially larger than that, thus encompassing both the matrix and the carbide phases. In this context also Vickers-to-Rockwell hardness conversions are not entirely reliable. Under low loads the converted HRC values tend to overestimate the actual Rockwell hardness [10]. Nevertheless, within each specimen group, the matrix hardness values were in general consistent and remained within the standard deviation, indicating good repeatability and measurement reliability.

The results of the nanoindentation tests performed on A-2 and B-2 specimens (bulk hardness of 49 ± 1 HRC) to assess the spatial hardness distribution across the microstructure are presented in Fig. 4. In the case of the hot work tool steel A, nanoindentation was targeted exclusively at the tempered martensite matrix. Figs. 4a and 4b show the location of the nanoindentation mapping for specimen A-2. while the corresponding hardness distribution map (Fig. 4c) reveals a uniform hardness profile across the entire analyzed area, with no pronounced local hardness variations. The average hardness across the mapped area was 5.8×10^3 MPa, corresponding to ~530 HV and 49 HRC, in good agreement with the bulk hardness measurement (Table 7).

In contrast, the cold work tool steel B (B-2), which contains a high volume fraction and high density of large, solidification derived Cr-rich carbides, exhibited a distinctly non-uniform hardness distribution. Figs. 4d and 4e show the location of the nanoindentation mapping for specimen B-2, while the hardness distribution map in Fig. 4f indicates hardness values ranging from approximately 5.4×10^3 MPa in the martensitic matrix to 18.1×10^3 MPa for the primary Cr-rich M_7C_3 carbides. The hardness of these massive solidification derived carbides typically ranged between 1.6×10^4 and 1.9×10^4 MPa (represented by the orange-red regions in Fig. 4f). The majority of the blue regions represent the matrix phase, with some hardness deviations due to secondary carbides or indents made near or at the carbide-matrix interface. Despite the pronounced local hardness heterogeneity, the average nanoindentation hardness of specimen B-2 remains consistent with the bulk hardness value of 49 HRC (Table 7).

Table 6
Matrix microhardness for the investigated tool steels at different hardness levels.

	Matrix hardness					
Specimen	A-1	A-2	A-3	B-1	B-2	B-3
HV0.05	647 ± 17	572 ± 5	496 ± 12	624 ± 9	549 ± 5	480 ± 11

3.4. Fracture toughness

In general, fracture toughness decreases with increased hardness. The same trend was observed within this investigation. However, for all the investigated hardness levels hot work tool steel A exhibited significantly higher fracture toughness (60 – 105%) as compared to cold work tool steel B. For the highest hardness level of 54 ± 1 HRC hot work tool steel (A-1) exhibited a fracture toughness of 39 MPa·m$^{1/2}$, while cold work tool steel (B-1) achieved only 24 MPa·m$^{1/2}$. At the intermediate hardness level of 49 ± 1 HRC, the hot work tool steel (A-2) reached a fracture toughness of about 70 MPa·m$^{1/2}$, and the cold work tool steel (B-2) roughly half of the A-2, about 34 MPa·m$^{1/2}$. As expected, the highest fracture toughness values were recorded in the lowest hardness group (45 ± 1 HRC). Here, the hot work tool steel (A-3) reached a fracture toughness of nearly 81 MPa·m$^{1/2}$, while the corresponding cold work tool steel (B-3) exhibited a value of 39 MPa·m$^{1/2}$.

The significantly lower fracture toughness values of the investigated cold work tool steel (1.2379 type) are largely attributed to its high volume fraction of coarse eutectic M_7C_3 carbides, which are inherently prone to cracking and contribute to the material's susceptibility to fracture initiation and propagation [26]. In contrast, such coarse carbides are absent in the investigated hot work tool steel (1.2367 type), which results in its superior fracture toughness [18].

3.5. Sliding wear resistance

3.5.1. Sliding wear resistance at high load (1.6 GPa)

The results of high-stress reciprocating sliding wear tests in the form of wear coefficient are presented in Fig. 6. In Fig. 6a for high-load and in Fig. 6b for low-load conditions. At high applied load of 102 N (1.6 GPa), cold work tool steel (B) for all three hardness levels consistently demonstrates lower sliding wear resistance against much harder Al_2O_3 counter-ball than hot work tool steel (A), as shown in Fig. 6a. It also displays higher coefficient of friction, especially for high hardness level, as shown in Fig. 7. Although hot work tool steel is virtually free of large solidification derived (M_7C_3) and secondary Cr-carbides ($M_{23}C_6$), present in high density in cold work tool steel, it displays more uniform microstructure with significantly higher fracture toughness at the same hardness levels. Its wear coefficient for high and medium hardness level (A-1, A-2) and high-load contact conditions is at about 0.6×10^{-5} mm^3 ·N^{-1} ·m^{-1}). However, as the hardness decreased to 45 HRC, the wear coefficient of hot work tool steel (A-3) increased, reaching its highest value of 1.0×10^{-5} mm^3 ·N^{-1} ·m^{-1}). This increase in wear at low hardness for large-carbides-free microstructure of hot work tool steel can be attributed to the onset of more significant plastic deformation due to the high applied load, compromising the material's resistance to sliding wear despite its higher fracture toughness. For cold work tool steel, the wear coefficient steadily increases with decreasing hardness (from $0.7.4 \times 10^{-5}$ mm^3·N^{-1}·m^{-1} at 54 HRC (B-1) to 1.30×10^{-5} mm^3 ·N^{-1} ·m^{-1} at 45 HRC (B-3)), showing up to 90% lower wear resistance than hot work tool steel, especially at intermediate hardness level

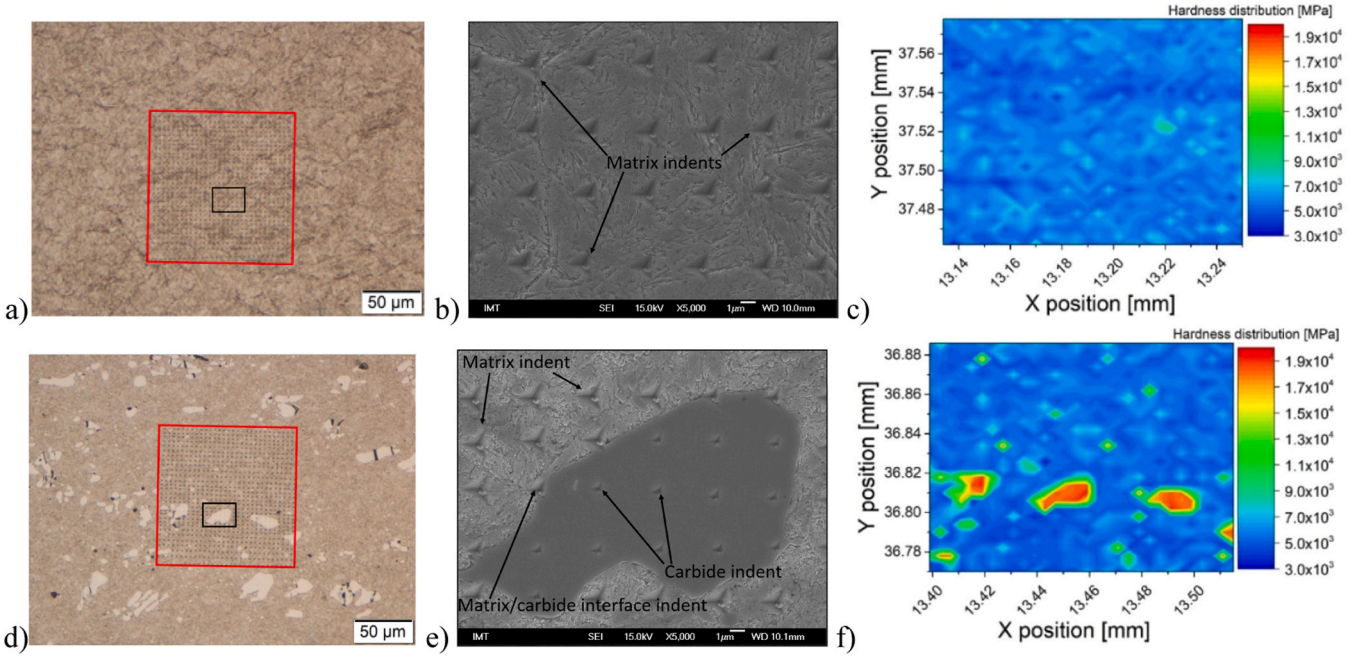

Fig. 4. Nanoindentation test results of the investigated tool steel specimens (a, b, c - A-2, d, e, f - B-2); a, d) optical micrograph of nanoindentaion site (red rectangle) and marked area of magnified SEI image (black rectangle), b, e) magnified SEM image in SEI mode showing sites of specific indents in the microstructure and c, f) nanoindentation hardness map (hardness distribution).

Table 7
Averaged nanoindentaion hardness values for the investigated specimens and corresponding HV and HRC values as provided by the nanoindentation software.

Specimen	IIM [MPa]		IIM [HV]		Rockwell [HRC] – bulk
A-2	5758 + /- 676		533 + /-62		49 + /- 0.15
B-2	Matrix	Carbide (M_7C_3)	Matrix	Carbide (M_7C_3)	49 + /-1.12
	5371 + /- 583	18089 + /- 803	498 + /- 54	1672 + /- 74	

*IIM – Instrumented Indentation method

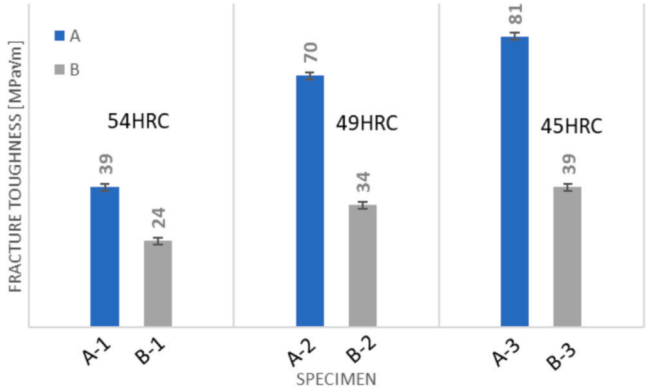

Fig. 5. Fracture toughness of the investigated tool steels at different hardness levels.

(B-2 vs. A-2).

Fig. 7 presents the initial stage of sliding, where it can be seen that steel B (Fig. 7a)—with the highest fraction and density of large eutectic M_7C_3 carbides—exhibits a markedly lower initial coefficient of friction (COF) as steel A (Fig. 7b) which is without large carbides. This can be attributed to the fact that hard carbide particles possess a lower local friction coefficient than the martensitic matrix and reduce the effective real contact area [19,32]. On the other hand steel A, which is dominated by the metallic matrix and contains only fine MC carbides, shows significantly higher initial friction due to a larger matrix–counterbody contact area and a greater tendency for early adhesion. As sliding progresses, surface evolution, plastic deformation, material transfer and tribofilm formation diminish these initial differences, leading both materials to converge toward a similar steady-state friction level.

The results of the average coefficient of friction during reciprocating sliding wear tests are presented in Fig. 8. In Fig. 8a for high-load and in Fig. 8b for low-load conditions. COF during reciprocating dry siding tests at the higher load was consistently lower for material A, ranging from 0.48 to 0.50, compared to material B, where COF values ranged from 0.50 to 0.55 (Fig. 8a). This lower COF for material A is likely related to its more uniform and ductile matrix, allowing for smoother sliding with less resistance.

3.5.2. *Sliding wear resistance at Low Load (1.0 GPa)*

When high-stress reciprocating sliding wear tests were performed at a considerably lower load of 30 N (1.0 GPa), the wear resistance trends for each tool steel remained unchanged. However, there was some difference when comparing both tool steels, particularly at higher hardness levels (Fig. 6b). At lower loads, the contribution of plastic deformation is reduced, making the plowing component more dominant, as also demonstrated by increased coefficient of friction (Fig. 8b). In this case, cold work tool steel at the highest hardness level (B-1) exhibited better wear resistance (2.1×10^{-5} $mm^3 \cdot N^{-1} \cdot m^{-1}$) than hot work tool steel (A-1), which primarily consists of a tempered martensitic matrix. This indicates that at very small plastic deformation presence of large hard carbides in hard matrix provide a significant contribution to wear resistance as well as friction level.

As the hardness decreased, cold work tool steel again displayed lower wear resistance than hot work tool steel. However, the difference was much smaller (<30%) than for high-load contact conditions and gradually increased with a drop in material hardness. For the lowest hardness level (3) wear coefficient of hot work tool steel (A-3) increased

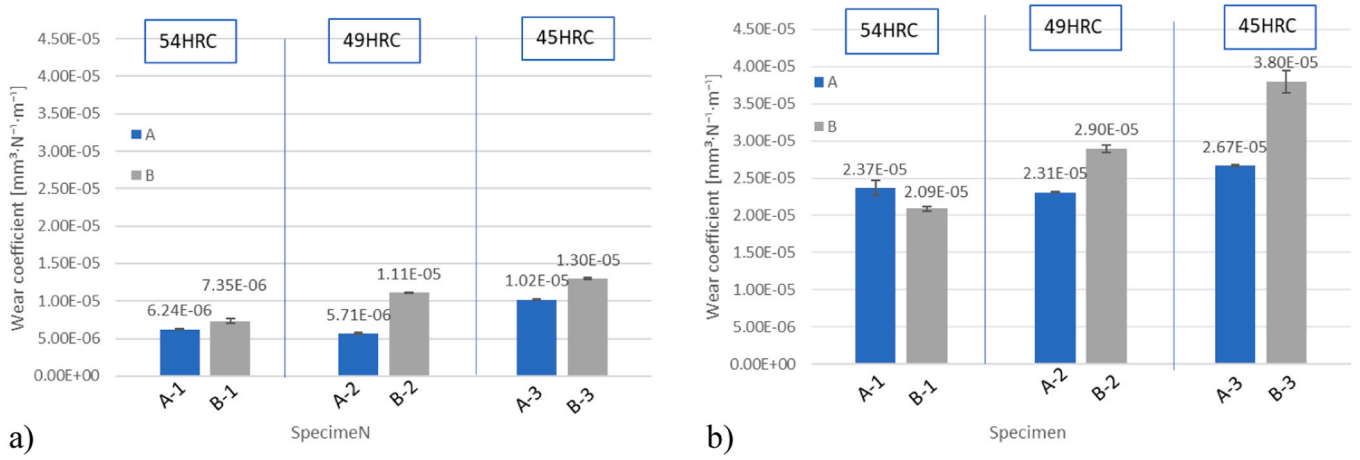

Fig. 6. Sliding wear resistance of investigated tool steels under reciprocating wear tests performed at (a) high load (102 N; 1.6 GPa) and (b) low load (30 N; 1.0 GPa).

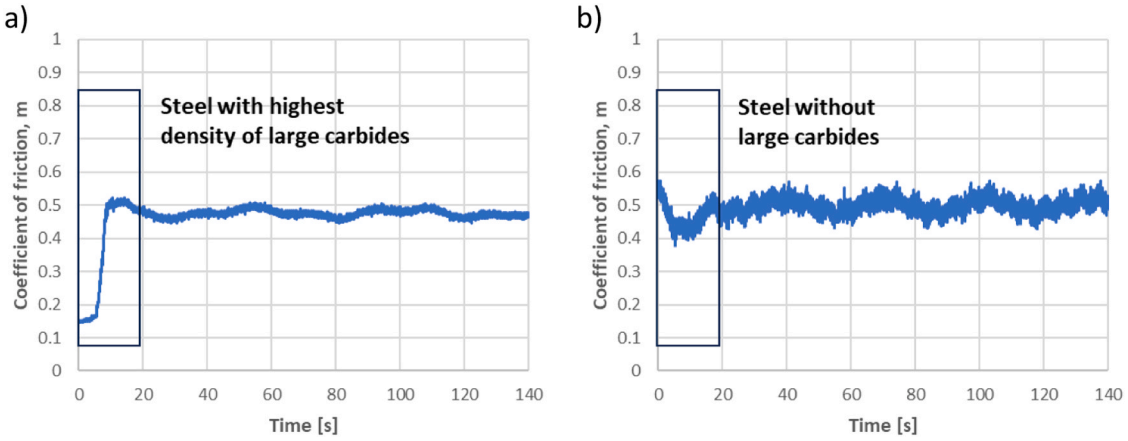

Fig. 7. COF during running-in at the high load sliding wear test of a) cold work tool steel B-2 (highest carbide fraction) and b) hot work tool steel A-2 (lowest carbide fraction).

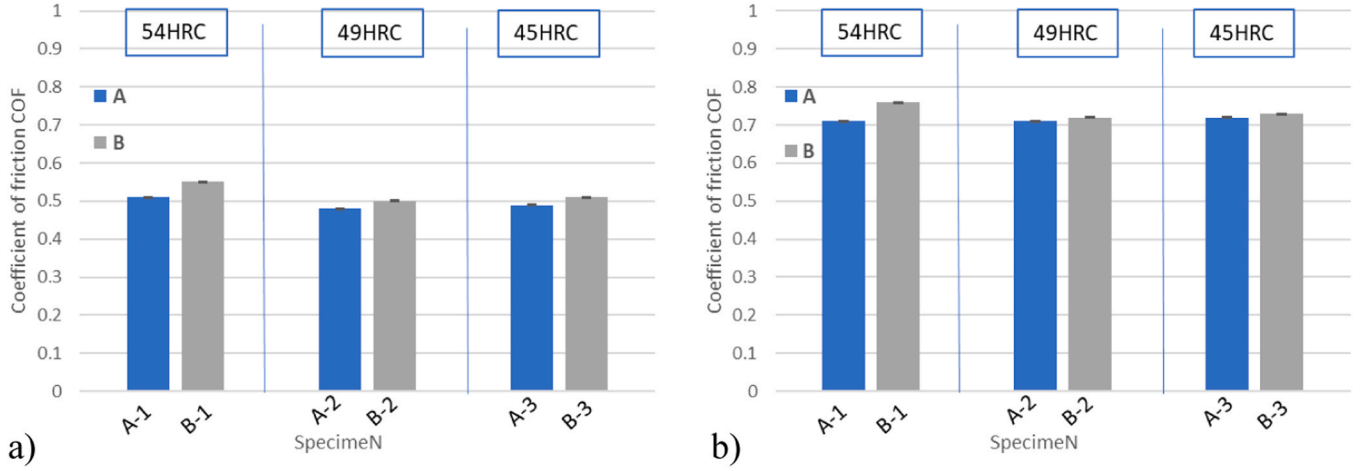

Fig. 8. Average coefficient of friction (COF) recorded during reciprocating dry siding wear tests at (a) high load (102 N; 1.6 GPa) and (b) low load (30 N; 1.0 GPa).

to 2.7×10^{-5} $mm^3 \cdot N^{-1} \cdot m^{-1}$, and for cold work tool steel (B-3) to 3.80×10^{-5} $mm^3 \cdot N^{-1} \cdot m^{-1}$ (Fig. 6b).

More pronounced wear of cold work tool steel, especially at lower hardness levels, indicates that a high fraction of large, hard carbides can actually compromise steel wear resistance when the matrix is too soft to support them. Although the carbides retain high hardness, the matrix with reduced hardness fails to provide load bearing support and adequately hold the large carbides in place, which can lead to their fracture and subsequent pull-out. The nanoindentation results confirmed significant hardness inhomogeneity in cold work tool steel (material B, Fig. 4), which supports the theory that, at insufficient matrix hardness, large carbides are no longer effectively supported and

anchored, promoting their detachment during wear and drop in coefficient of friction. Similar findings were reported by [33], where PM and MIM-prepared composites containing VC carbides exhibited lower wear coefficients at intermediate carbide fractions. Higher carbide contents led to larger carbide precipitates with weaker adhesion to the matrix, increasing the likelihood of carbide pull-out and third-body abrasion.

At high contact stresses and more pronounced plastic deformation the wear mechanisms become more complex. Although two materials (material A and B can have similar bulk hardness, the difference in microstructure composition and associated properties like fracture toughness, ductility, and yield strength become the decisive factor.

As can be seen on Fig. 8b, COF values increased significantly to approximately 0.7 and above. This effect was consistent across specimens, with COF values around 0.71–0.76, slightly higher for specimen B-1. The increased COF at lower loads and high speeds could be attributed to the reduced contribution of plastic deformation and the increased role of micro-roughness and carbide protrusions in the sliding contact.

3.5.3. *Influence of plastic deformation and fracture toughness*

In the case of hot work tool steel (material A), which lacks large carbides, plastic deformation plays a significant role, but this deformation appears to contribute to material's overall wear resistance, shear strength and friction level under high-stress conditions. This is most probably due to uniform energy dissipation mechanisms and higher fracture toughness supporting the material's integrity. In contrast, cold work tool steel (material B) shows less plastic deformation under the same contact conditions, but more efficient material removal via plowing and scratching with higher friction. These wear modes predominate because the matrix cannot sufficiently support and retain large carbides, which are easily dislodged and act as third-body abrasive wear particles. This is further supported by wear behavior at lower loads.

At 30 N and 54 HRC, cold work tool steel shows superior wear resistance due to the dominance of the carbides in resisting abrasive action, and absence of large plastic deformation. At 30 N, contact stresses (1000 MPa) remain well below the yield strength (1500 – 1600 MPa) of both materials (A-1 & B-1). However, as hardness decreases, the ability of the matrix in cold work tool steel (B-2 & B-3) to support the carbides at increased plastic deformation diminishes, leading to a sharp increase in wear. In contrast, for hot work tool steel (A-2 & A-3) the absence of coarse carbides and much higher fracture toughness result in only minimal change in wear resistance at reduced material hardness.

This highlights the trade-off between carbide-driven abrasive wear resistance and the negative impact of large carbides on fracture toughness, which is crucial for applications with combined mechanical loading and abrasive wear conditions.

3.5.4. *Role of carbides as third-body particles*

As discussed, detached carbides can significantly influence wear behavior of the material, particularly when acting as third-body abrasive wear particles [32]. During reciprocating sliding, wear particles mainly tend to accumulate along the edges of the wear track. However, especially under dry sliding they may also remain partially trapped within the contact and act as third bodies, changing wear mechanism form two-body to more severe three-body abrasive wear. To further investigate this effect, a dedicated set of experiments involving in-situ removal of any generated wear particles through air blowing was conducted at high speed/high-stress (30 N, 1 GPa) contact conditions. The key question addressed was whether the accumulation of detached carbides within the contact zone of tool steel leads to a transition from two-body to three-body abrasive wear and intensified wear process.

As shown in Fig. 9, the difference in friction, wear severity and wear coefficient for the hot work tool steel (material A) was negligible when comparing tests with and without in-situ wear particles removal. Wear coefficient with wear particles removal was less than 4% lower as for the conventional reciprocating sliding tests. This minimal difference indicates that in the case of hot work tool steel which is free of large coarse carbides, trapped wear particles have only negligible effect without any third-body abrasive action. The predominant wear mechanism remains governed by plastic deformation and micro-plowing.

In contrast, for the cold work tool steel (material B), which contains a high volume fraction of large Cr-rich carbides, removal of wear particles led to a significantly different response. Wear coefficient for cold work tool steel at the highest hardness level (B-1) dropped from 2.1×10^{-5} $mm^3 \cdot N^{-1} \cdot m^{-1}$, to less than 1.6×10^{-5} $mm^3 \cdot N^{-1} \cdot m^{-1}$ when wear particles were actively removed from the contact during testing. This represents a drop in wear coefficient of about 25%. The results confirm that for carbide-rich tool steels, detached carbides play an important role in promoting and intensifying abrasive wear through third-body abrasion if not efficiently removed from the contact area. However, no change in friction could be detected (Fig. 9b), confirming abrasive wear as the main wear mechanism in both cases.

Those results clearly show that in carbide-rich tool steels detachment and accumulation of wear particles can have a substantial effect on the wear process, while in steels with low carbide fractions in wear process is mainly influenced by the intrinsic properties of the matrix.

3.6. *Wear tracks investigation*

Scanning Electron Microscopy (SEM) of the wear tracks including subsurface microstructural examination revealed differences in wear

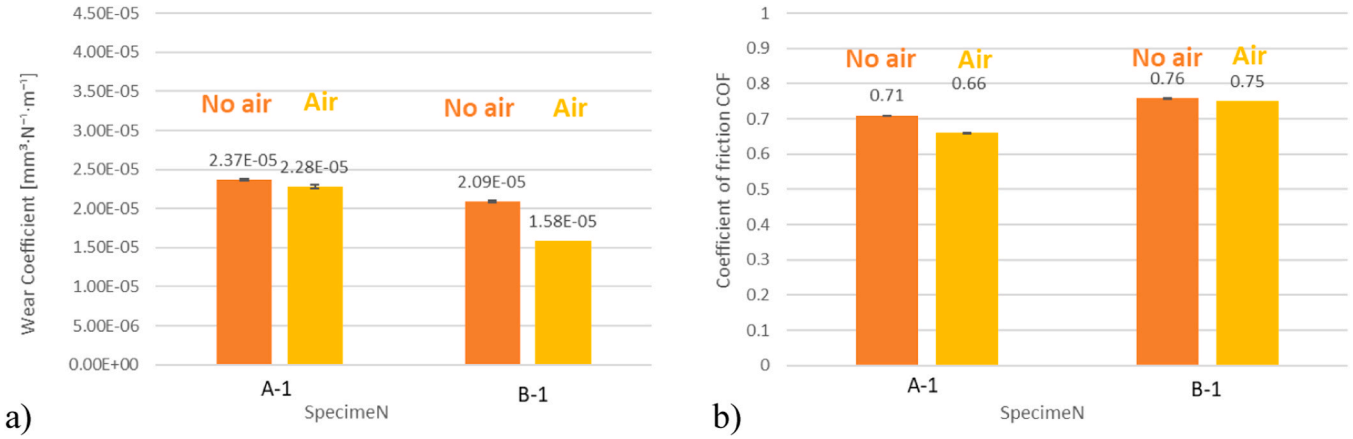

Fig. 9. Effect of in-situ wear particles removal on (a) wear coefficient and (b) coefficient of friction of A-1 and B-1 test specimens during reciprocating dry sliding test (0.12 m/s, 1 GPa).

and damage mechanisms depending on the material type (type, size and fraction of carbides) and test conditions. Representative SEM images for the reciprocating dry sliding wear tests are shown in Fig. 10 and Fig. 11. All wear tracks show a mixed-mode sliding wear response, in which abrasion represents only part of the overall behavior. Depending on the carbide fraction, carbide size, and matrix hardness, the surfaces also show evidence of plastic deformation, brittle carbide fracture, subsurface fatigue damage and delamination, as well as tribochemical and oxidative processes. In Fig. 10 for the investigated tool steels at the highest hardness level of 54 HRC and in Fig. 11 at the lowest hardness of 45 HRC. In the case of cold work tool steel with large solidification derived carbides and high fraction of carbides hardened to 54 HRC (B-1; Fig. 10a), cracking, partial smoothening and detachment of those large carbides can be observed, with visible voids around some of the detached carbides. It is important to note that tool steels containing coarse solidification derived carbides typically exhibit pre-existing cracks within these carbides, with the sliding contact further accelerating their fracturing and eventual detachment. Additionally, several larger craters, indicative of material removal, can be observed on the worn surface. Some degree of plastic deformation was also evident in the microstructure.

In contrast, the worn surface of hot work tool steel (A-1; Fig. 10b), which has a much finer carbides and lower carbide fraction at the same hardness level, shows considerably smoother and flatter appearance, though some larger abrasion grooves are still present. The surface morphology indicates that plastic deformation is more pronounced in this material, aligning with its lower carbide content and higher fracture toughness.

When the same materials were tested under lower applied load (30 N; Figs. 10c and 10d), a more pronounced abrasive wear pattern was observed and degree of plastic deformation reduced. Furthermore, as shown in Fig. 10c, carbides cracking and removal has been reduced for cold work tool steel. The worn surface of hot work tool steel (A-1) tested under lower load conditions (Fig. 10d) displays characteristic short shallow scratches, which can be associated with the effect of small MC carbides present in its microstructure. The behavior of these fine carbides under sliding conditions was thoroughly described in our previous work [34].

At reduced hardness levels cold work tool steel (B-3) exhibited severely damaged wear surfaces regardless of the load applied in wear testing, as shown in (Figs. 11a and 11c). The worn surfaces are rough, with significant material removal, large craters, and majority of large carbides being cracked and removed. This confirms the inability of softer matrix to provide adequate load bearing capacity and support large carbides, which are rapidly fractured and detached during sliding.

In contrast, hot work tool steel (A-3; Figs. 11b and 11d) continues to exhibit smoother wear tracks with signs of pronounced plastic deformation, especially at high loads. The wear scar morphology indicates that, despite lower hardness, large-carbides-free hot work tool steel can undergo substantial plastic flow without experiencing severe wear and material removal, observed in cold work tool steel. This highlights the influence of microstructural characteristics, specifically carbide size and distribution, on the dominant wear mechanism and wear resistance of tool steels.

Cross-section microstructural analysis of unidirectional sliding wear track for low hardness group specimens (45 HRC), aimed at revealing wear mechanism and damage evolution is shown in Fig. 12 (1.2379; B-3) and Fig. 12 (mod. 1.2367; A-3). In the case of high-carbon, high-chromium cold work tool steel (1.2379; B-3) initial unworn and undeformed microstructure consists of undamaged large M_7C_3 Cr-rich solidification derived carbides and small $M_{23}C_6$ Cr-rich secondary carbides, all encapsulated within a tempered martensitic matrix (Fig. 12a). After being subjected to unidirectional sliding against a much harder counter-ball (Al_2O_3), a severely damaged subsurface region develops. As shown in Figs. 12b and 12c, cracked as well as highly fragmented large solidification derived carbides can be seen in the contact zone. Elongated carbides located at the contact surface get crushed into smaller fragments by being trapped between the hard counter-body and another hard carbide particle beneath. Furthermore, as the martensitic matrix beneath the wear track undergoes plastic deformation under sliding, the

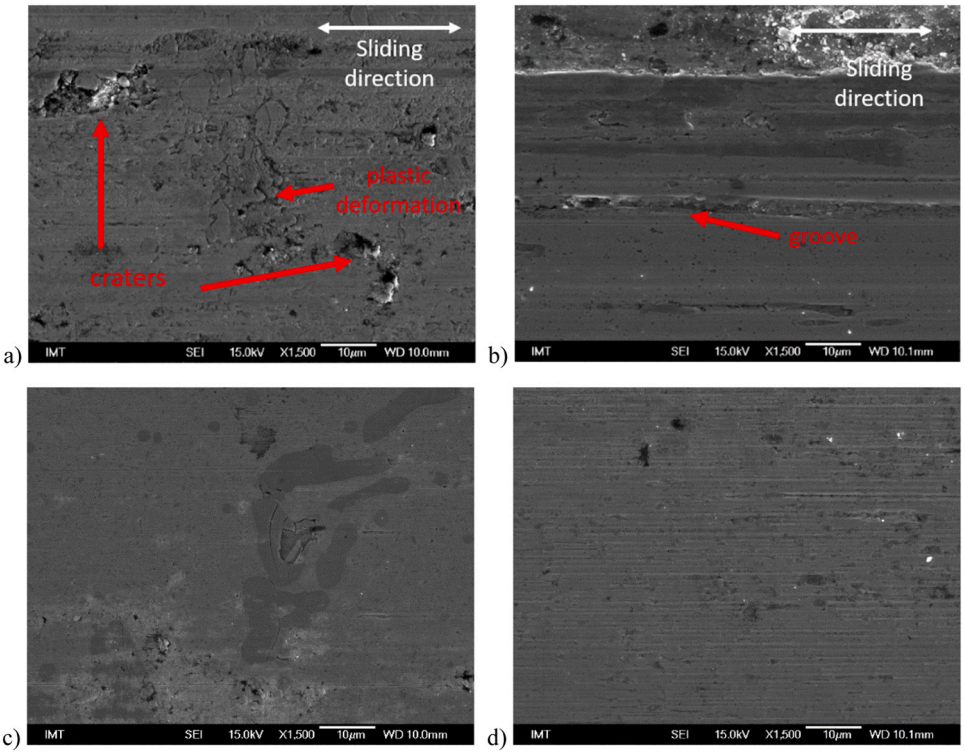

Fig. 10. Top view SEM micrographs of reciprocating sliding wear track for a, c) cold work tool steel (B-1) and b, d) hot work tool steel (A-1) hardened to 54 HRC; a, b) $p_H = 1.6$ GPa and c, d) $p_H = 1.0$ GPa (white arrow indicates reciprocating sliding direction).

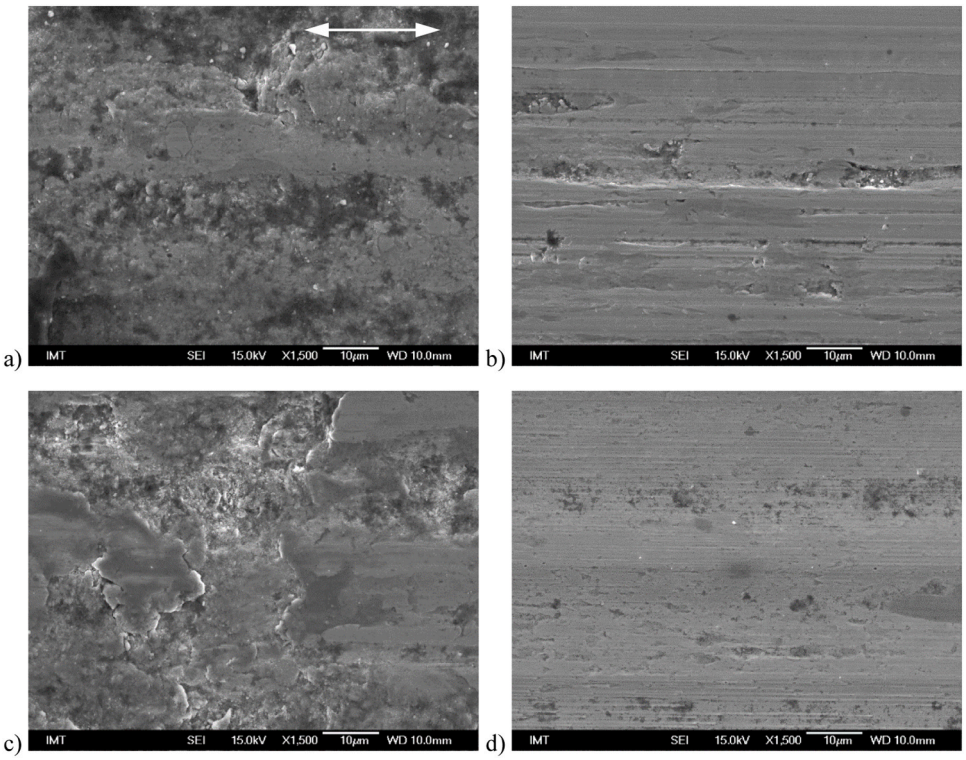

Fig. 11. Top view SEM micrographs of reciprocating sliding wear track for a, c) cold work tool steel (B-3) and b, d) hot work tool steel (A-3) hardened to 45 HRC; a, b) $p_H = 1.6$ GPa and c, d) $p_H = 1.0$ GPa (white arrow indicates reciprocating sliding direction).

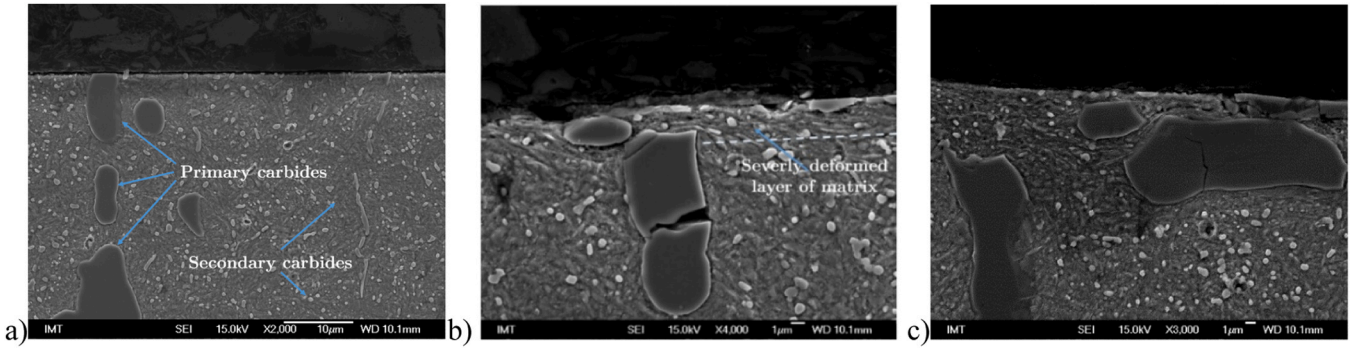

Fig. 12. Microstructure cross-section view of cold work tool steel hardened to 45 HRC (B-3); (a) unworn surface and (b-c) wear track after 200 m of unidirectional sliding against Al_2O_3 counter-ball @1.0 GPa.

embedded large carbides with a significantly lower ductility than the surrounding matrix become highly stressed, leading to their fracturing.

Due to high volume fraction and presence of large carbides plastic deformation of the matrix is limited to the region immediately beneath the wear track (3–5 μm), while the matrix further away from the contact zone remains unaffected. This effectively "pins" large carbides from the bottom side while dynamic loading during sliding promotes their fracture, movement and eventual dislodgment at the worn surface, as illustrated in Fig. 12b. In addition to carbide cracking, matrix cracking is also observed, particularly in areas close to the larger carbides and near the worn surface. Process of large carbides cracking, rearrangement with matrix plastic flow and displacement (Fig. 12) leads to the formation of voids deep beneath the worn surface, further reducing the structural integrity of the material and increasing its susceptibility to wear.

Smaller secondary carbides, on the other hand retain their structural integrity and follow plastic deformation of the tempered martensitic matrix, as shown in Figs. 12b and 12c. This difference in behavior between large and small carbides highlights the crucial role of carbides size and distribution in terms of tool steel wear response.

Contrary to cold work tool steel (1.2379; B-3), microstructure of hot work tool steel (mod. 1.2367; A-3) consists predominantly of tempered martensite with a very low fraction of fine, sparsely distributed MC V-rich carbides (Fig. 13a). When this material is subjected to high-stress sliding wear (1 GPa), using the same contact pressure as applied for sample B-3, it shows a markedly different subsurface response with a substantial shear and plastic deformation, as shown in Figs. 13b and 13c. The cross-section analysis of specimen A-3 reveals that under high-stress sliding the tempered martensitic structure undergoes substantial compression and bending of the martensite laths in the direction of sliding. This is a key difference compared to large-carbides dominated microstructure of cold work tool steel (B-3), where carbide cracking and detachment dominate the damage mechanism.

Notably, for large-carbides-free hot work tool steel very few carbide particles were observed beneath the worn surface (Figs. 13b and 13c). This confirms that the material's wear response is primarily governed by the ductility and plastic flow of the tempered martensite, with limited

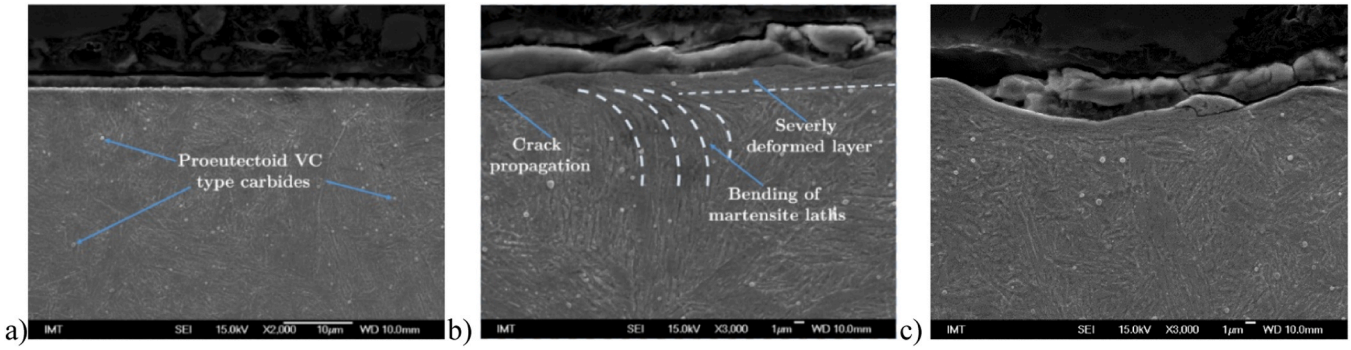

Fig. 13. Microstructure cross section view of hot work tool steel hardened to 45 HRC (A-3); (a) unworn surface and (b, c) wear track after 200 m of unidirectional sliding against Al2O3 counter-ball 1.0 GPa.

contribution from hard carbides interactions. The absence of a significant carbide population likely contributes to the smoother, more plastically deformed wear track morphology (Fig. 11d).

4. Conclusions

Results of this study, aimed at determining the effect and role of carbides in high-stress sliding wear behaviour of tool steels can be summarized in the following conclusions:

At the same bulk hardness level hot work tool steel mod. 1.2367 with the microstructure mainly consisting of tempered martensite with finely dispersed small MC carbides shows very uniform microhardness distribution and up to two-times better fracture toughness than cold work tool steel 1.2379, characterized by high carbides density and large coarse solidification derived carbides.

In general, material's bulk hardness defines the level of sliding wear resistance. Higher hardness resulting in lower wear coefficient. However, as demonstrated by this study it is not only about inherent material hardness. Wear performance of tool steels is strongly influenced by carbide fraction, size, and matrix load-bearing capacity.

Large coarse carbides, if not sufficiently supported by a hard matrix, are prone to fracture, fragmentation and detachment, which can significantly reduce wear resistance, especially at low hardness levels with insufficient matrix hardness. In this respect, matrix strength has a crucial role in maintaining carbide integrity during sliding wear.

Generated wear particles and carbide fragments further contribute to increased wear by introducing hard third-body particles into the contact and leading to more severe abrasive conditions. This effect is particularly detrimental when large carbide fragments remain trapped in the contact zone, highlighting the importance of material dynamic behavior under stress and wear particles interaction.

The interplay between matrix hardness, carbide fraction, size, and type critically dictates the wear behavior of tool steels. Contact condition based balance between these microstructural features, ensuring sufficient matrix support and controlled carbide characteristics is essential for best wear performance.

CRediT authorship contribution statement

Marko Sedlaček: Writing – original draft, Supervision, Investigation, Data curation, Conceptualization. **Božo Skela:** Writing – original draft, Validation, Investigation, Formal analysis, Conceptualization. **Podgornik Bojan:** Writing – review & editing, Supervision, Resources, Conceptualization.

Declaration of Competing Interest

The authors declare the following financial interests/personal relationships which may be considered as potential competing interests: Marko Sedlacek reports financial support was provided by Slovenian Research and Innovation Agency. If there are other authors, they declare that they have no known competing financial interests or personal relationships that could have appeared to influence the work reported in this paper.

Acknowledgements

This work was done in the frame of the research program P2–0050 which is financed by the Slovenian Research Agency. The author would also like to thank Slovenian national building and civil engineering institute (Laboratory for Metals, Corrosion and Anticorrosion protection) for the use of TRIBOtechnic Pin-on-Disc TRIBOtester and performing unidirectional sliding wear tests.

Data availability

https://doi.org/10.5281/zenodo.18162435

References

[1] Wei MX, Wang SQ, Wang L, Cui XH, Chen KM. Effect of tempering conditions on wear resistance in various wear mechanisms of H13 steel. Tribol Int 2011;44(7–8):898–905.
[2] Tekeli S, Güral A. Dry sliding wear behaviour of heat treated iron based powder metallurgy steels with 0.3% Graphite+ 2% Ni additions. Mater Des 2007;28(6):1923–7.
[3] Sapate SG, Chopde AD, Nimbalkar PM, Chandrakar DK. Effect of microstructure on slurry abrasion response of En-31 steel. Mater Des 2008;29(3):613–21.
[4] Totten GE. Steel heat treatment: metallurgy and technologies. crc Press; 2006.
[5] Højerslev C. Tool steels. Risø National Laboratory. Denmark: Forskningscenter Risoe; 2001. Risoe-R No. 1244(EN).
[6] Fukaura K, Yokoyama Y, Yokoi D, Tsujii N, Ono K. Fatigue of cold-work tool steels: effect of heat treatment and carbide morphology on fatigue crack formation, life, and fracture surface observations. Met Mater Trans A 2004;35(4):1289–300.
[7] Badisch E, Mitterer C. Abrasive wear of high speed steels: influence of abrasive particles and primary carbides on wear resistance. Tribol Int 2003 Oct;36(10):765–70.
[8] Bergman F, Hedenqvist P, Hogmark S. The influence of primary carbides and test parameters on abrasive and erosive wear of selected PM high speed steels. Tribol Int 1997 Mar;30(3):183–91.
[9] Kirkhorn L, Bushlya V, Andersson M, Ståhl JE. The influence of tool steel microstructure on friction in sheet metal forming. Wear 2013 Apr;302(1–2):1268–78.
[10] Das D, Dutta AK, Ray KK. Influence of varied cryotreatment on the wear behavior of AISI D2 steel. Wear 2009;266(1–2):297–309.
[11] Singh K, Khatirkar RK, Sapate SG. Microstructure evolution and abrasive wear behavior of D2 steel. Wear 2015;328:206–16.
[12] Arain A. Heat treatment and toughness behavior of tool steels (D2 and H13) for cutting blades. Natl Libr Can= Biblio{è}Que Natl du Can 1999.
[13] Ko DC, Kim SG, Kim BM. Influence of microstructure on galling resistance of cold-work tool steels with different chemical compositions when sliding against ultra-high-strength steel sheets under dry condition. Wear 2015;338:362–71.
[14] Gåård A, Hallbäck N, Krakhmalev P, Bergström J. Temperature effects on adhesive wear in dry sliding contacts. Wear 2010;268(7–8):968–75.
[15] Berns H. Microstructural properties of wear-resistant alloys. Wear 1995;181:271–9.
[16] Casellas D, Caro J, Molas S, Prado JM, Valls I. Fracture toughness of carbides in tool steels evaluated by nanoindentation. Acta Mater 2007;55(13):4277–86.

[17] Bahrami A, Anijdan SHM, Golozar MA, Shamanian M, Varahram N. Effects of conventional heat treatment on wear resistance of AISI H13 tool steel. Wear 2005; 258(5–6):846–51.
[18] Leskovšek V, Šuštaršič B, Jutriša G. The influence of austenitizing and tempering temperature on the hardness and fracture toughness of hot-worked H11 tool steel. J Mater Process Technol 2006;178(1):328–34.
[19] Hutchings I, Shipway P. Tribology Frict wear Eng Mater Second Ed 2017.
[20] Zum Gahr KH. Microstructure and wear of materials (editor.). Amsterdam New York: Elsevier; 2010. p. 560 (editor.).
[21] Bryson W.E., Bryson W.E. Heat treatment, selection, and application of tool steels. 2005;
[22] Leskovšek V, Podgornik B. Tool steels: Fracture Toughness. Encylopedia of Iron, Steel, and Their Alloys. New York: Taylor and Francis; 2016. p. 3687–719.
[23] Blaha J, Krempaszky C, Werner E, Liebfahrt W. Carbide distribution effect in cold work tool steels. Proc 6th Int Tool Conf 10-13, 2002; Sept 2002. p. 289–98.
[24] Delagnes D, Lamesle P, Mathon MH, Mebarki N, Levaillant C. Influence of silicon content on the precipitation of secondary carbides and fatigue properties of a 5%Cr tempered martensitic steel. Mater Sci Eng A 2005 Mar;394(1–2):435–44.
[25] Roberts GA, Krauss G, Kennedy R. Tool steels. 5th ed. Materials (editors.). Park, OH: ASM International; 2010. p. 364 (editors.).
[26] Viale D, Béguinot J, Chenou F, Baron G. Optimizing microstructure for high toughness cold-work tool steels. Proc 6th Int Tool Conf 2002:299–318.
[27] Bhadeshia HKDH, Honeycombe RWK. Steels: microstructure and properties. Fourth edition. Amsterdam Boston Heidelberg London New York Oxford Paris San Diego San Francisco Singapore Sydney Tokyo: Elsevier, Butterworth-Heinemann; 2017. p. 1.
[28] Thomson RC, Miller MK. Carbide precipitation in martensite during the early stages of tempering: Cr- and Mo-containing low-alloy steels. Acta Mater 1998;46: 2203–13. https://doi.org/10.1016/S1359-6454(97)00420-5.
[29] Roberts GA, Krauss G, Kennedy R. Tool steels. 5th ed. Materials Park, OH: ASM International; 2010. p. 364 (editors.).
[30] Sjöström J. Chromium martensitic hot-work tool steel: damage, performance and microstructure. Karlstad: Univ; 2004. p. 53.
[31] Cui XH, Wang SQ, Wei MX, Yang ZR. Wear Characteristics and Mechanisms of H13 Steel with Various Tempered Structures. J Mater Eng Perform 2011 Aug;20(6): 1055–62.
[32] Gwidon Stachowiak, Andrew W. Batchelor, Engineering Tribology. 4th Edition. Butterworth-Heinemann; August 19, 2016. , ISBN: 9780128100318.
[33] García C, Martín F, Herranz G, Berges C, Romero A. Effect of adding carbides on dry sliding wear behaviour of steel matrix composites processed by metal injection moulding. Wear 2018 Nov;(414–415):182–93.
[34] Skela B, Sedlaček M, Kafexhiu F, Podgornik B. Wear behaviour and correlations to the microstructural characteristics of heat treated hot work tool steel. Wear 2019 Apr;426–427:1118–28.